SUPPORTING INFORMATION

Chinese Journal of Structural Chemistry

Atomically Thin 2D TiO_2 Nanosheets with Ligand Modified Surface for Ultra-sensitive Humidity Sensor

Jianze Xiao[1,2], Zhihua Fu[2], Guane Wang[2,3], Xiaoliang Ye[2]* and Gang Xu[2,3,4]*

[1]*College of Chemistry, Fuzhou University, Fuzhou 350116, China*

[2]*State Key Laboratory of Structure Chemistry, Fujian Institute of Research on the Structure of Matter, Chinese Academy of Science, Fuzhou 350002, China*

[3]*University of Chinese Academy of Sciences, Beijing 100049, China*

[4]*Fujian Science & Technology Innovation Laboratory for Optoelectronic Information of China, Fuzhou 350108, China*

Corresponding authors. Emails: gxu@fjirsm.ac.cn (Gang Xu;) and yexl@fjirsm.ac.cn (Xiaoliang Ye)

n EXPERIMENTAL

Chemicals and Materials. All chemical reagents used in this work were obtained commercially. Unless otherwise noted, all the reagents were of analytical grade and used without further purification. Titanium tetrachloride ($TiCl_4$, 99.0%) was purchased from Shanghai Macklin Biochemical Co., Ltd. (China). Ethylene glycol (CH_2OH-CH_2OH, EG), ethylenediamine (CH_2NH_2-CH_2NH_2, EA), sodium oxalate (OA-Na), and absolute ethanol (CH_3CH_2OH) were obtained from Sinopharm Chemical Reagent Co., Ltd. (China). Deionized (DI) water used in all experiments was prepared from the Milli-Q water purification system with a resistivity of 18.2 MΩ·cm. Sensor substrates (Al_2O_3) with 5 pairs of Ag−Pd interdigitated electrodes with a channel of 200 μm were purchased from Beijing Elite Tech Co. (China). The sensor substrates were rinsed with ethanol and dried with nitrogen before drop-casting.

Synthesis of TiO_2-EG Ultra-thin Nanosheets. The TiO_2-EG ultra-thin nanosheets were synthesized via a modified solvothermal method reported by Wang's group.[1] In a typical synthesis of TiO_2-EG ultra-thin nanosheets, 1 mL $TiCl_4$ and 30 mL EG were mixed and magnetically stirred for 5 min till no HCl yield. Then 1 mL DI water was added into the mixture solution and the resulting light yellow homogeneous solution was allowed to react at 160 °C for 6 hours in a 50-mL Teflon-lined stainless-steel autoclave before it cooled to room temperature naturally. The white products were collected after centrifugation and further washed three times with DI water and absolute ethanol. After being dried in a 60 °C vacuum oven overnight, the collected TiO_2-EG powder was used for characterizations, humidity sensing tests, and further synthesis.

Synthesis of TiO_2-EA Ultra-thin Nanosheets. The TiO_2-EA ultra-thin nanosheets were synthesized, followed by a facile post-ligand modification strategy. Briefly, 110 mg TiO_2-EG and 100 mL DI water were mixed in a 250 mL round-bottom flask, and then 4 mL ethylenediamine (EA) was introduced into the mixture solution. The 250 mL round-bottom flask was transferred to an oil bath at 50 °C and magnetically stirred for 6 hours. The sandy beige products were collected after centrifugation and washed three times with DI water and absolute ethanol. After being dried in a 60 °C vacuum oven overnight, the collected TiO_2-EA powder was used for characterizations and humidity sensing tests.

Synthesis of TiO_2-OA Ultra-thin Nanosheets. The synthetic process of TiO_2-OA ultra-thin nanosheets was similar to TiO_2-EA ultra-thin nanosheets. 110 mg TiO_2-EG and 100 mL DI water were mixed in a 250 mL round-bottom flask, and then 0.4 g sodium oxalate (OA-Na) was introduced into the mixture solution. The 250 mL round-bottom flask was transferred to an oil bath at 50 °C and magnetically stirred for 6 hours. The white products were collected after centrifugation and washed three times with DI water and absolute ethanol. After being dried in a 60 °C vacuum oven overnight, the collected TiO_2-OA powder was used for characterizations and humidity sensing tests.

Sensor Device Fabrication. The gas sensor devices were fabricated by a typical drop-casting method. Initially, a proper amount of prepared sensing material was mixed with absolute ethanol and ground in an agate mortar to form a slurry. Then the slurry was coated on pre-cleaned Ag-Pd interdigitated electrodes in which Al_2O_3 ceramic was used as sensor substrate. The coated slurry was dried naturally to form a uniform thin film sensing layer at room temperature. And two gold wires were attached to each side of the interdigitated electrodes via a silver conductive paste. Then sensor devices were aged in a vacuum oven at 80 °C for 6 hours before sensing test. The sensor devices of TiO_2-EG, TiO_2-EA, and TiO_2-OA were fabricated with the same method mentioned above.

Humidity Sensing Performance Test. The humidity sensing performance of sensor devices was measured through the homemade sensing test system that we have reported.[2] The sensor devices were placed in a dark sealed quartz chamber and dry synthetic air was used as the carrier gas for humidity. DC circuit method was adopted to evaluate the humidity sensing performance of sensor devices. The DC changes were recorded using a Keithley 2602B Source meter when sensor devices were exposed to different relative humidity with an applied bias of 1 V. Humid gas was introduced into the quartz chamber with a flow rate of 12–600 mL min^{-1} via mass flow controllers. The flow and relative humidity could be controlled by using the mass flow controllers (MFC). All of the humidity sensing measurements were performed at an ambient condition.

The response time is defined as the time taken by the fabricated sensor to reach 90% of the response value upon exposure to the target humidity, while the recovery time is defined as that taken by the fabricated sensor to decrease 90% of the response value upon exposure to the dry air.

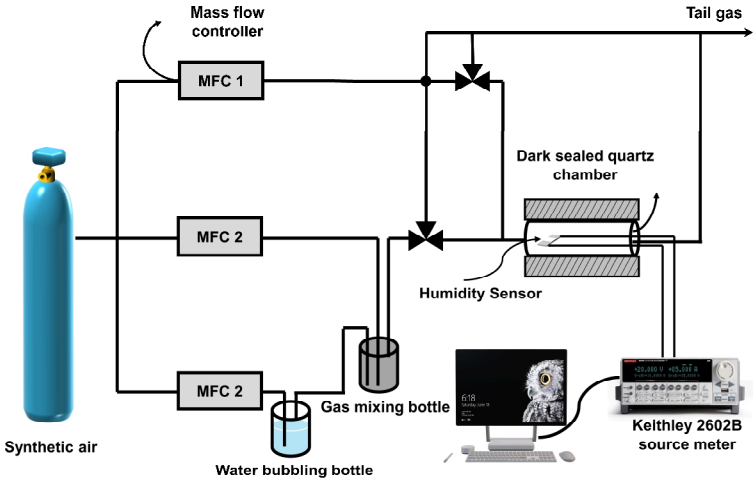

Home-made humidity sensing test system

Materials characterization. Powder X-ray diffraction (PXRD) test was performed by using Rigaku SmartLab diffractometers (Japan) with a CuKα radiation (λ = 1.5418 Å). The 2θ diffraction angle range was from 5 to 80° with a scanning speed of 5 °·min^{-1}. Fourier transform infrared spectroscopy (FT-IR) measurements were conducted with a Bruker VERTEX 70 FTIR spectrometer (Germany) using KBr tablets over the wavenumber range from 4000 to 400 cm^{-1}. The X-ray photoelectron spectroscopy (XPS) was tested by a Thermo Scientific ESCALAB 250 Xi XPS system (monochromatic AlKα X-ray (1486.6 eV) operating at 15 kV; the base pressure: 5.0 × 10−8 Pa). The samples were dried in a vacuum oven for 8 h before XPS tests. The morphology details of TiO_2-EG, TiO_2-EA, and TiO_2-OA were observed by scanning electron microscope (SEM, Zeiss Sigma-300) and field emission transmission electron microscope (FETEM, Tecnai F20). Atomic force microscope (AFM) images were collected on a Bruker Dimension ICON atomic force microscope. The scanning was performed under the ScanAsyst in air mode with a scanning force of the tip on the surface. Nitrogen adsorption isotherms of TiO_2-(EG, EA, OA) nanosheets were measured using a Micromertics ASAP 2020 gas adsorption analyzer at 77 K, and samples were degassed at 100 °C for 8 hours. The BET method was used to calculate the specific surface area ($m^2 \cdot g^{-1}$). The UV-vis-NIR spectroscopy was measured by a PerkinElmer Lambda-900 UV-vis-NIR spectrophotometer.

n FIGURES AND TABLES

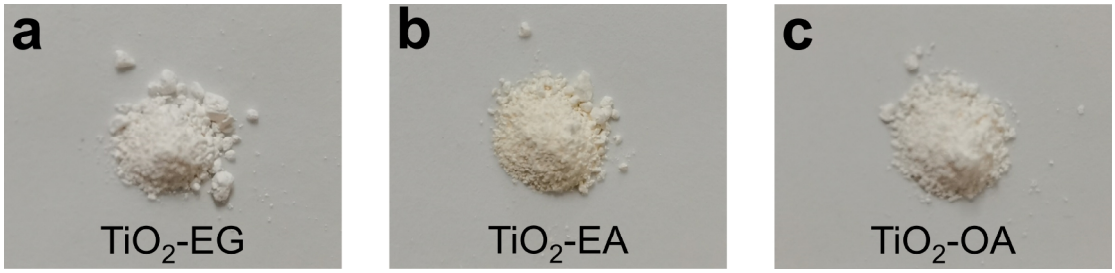

Figure S1. Optical images of (a) TiO_2-EG, (b) TiO_2-EA, and (c) TiO_2-OA.

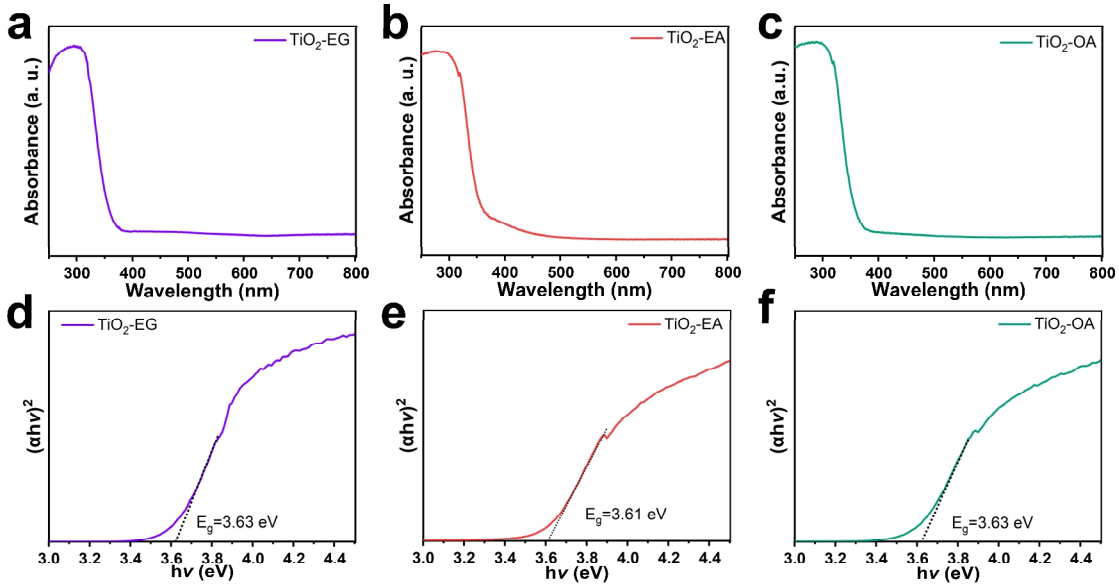

Figure S2. UV-vis-NIR spectroscopy and corresponding optical band gap of (a, d) TiO_2-EG, (b, e) TiO_2-EA, and (c, f) TiO_2-OA.

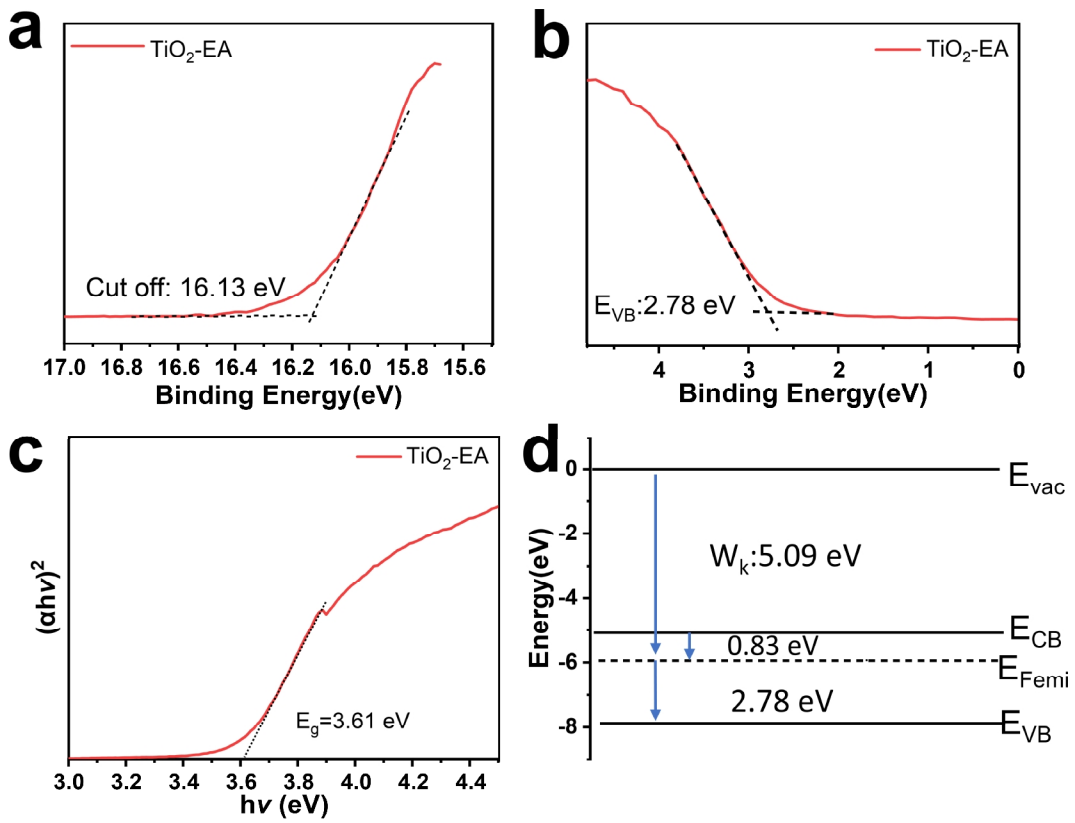

Figure S3. (a), (b) UPS spectrum, (c) optical band gap and (d) energy level plot of TiO_2-EA.

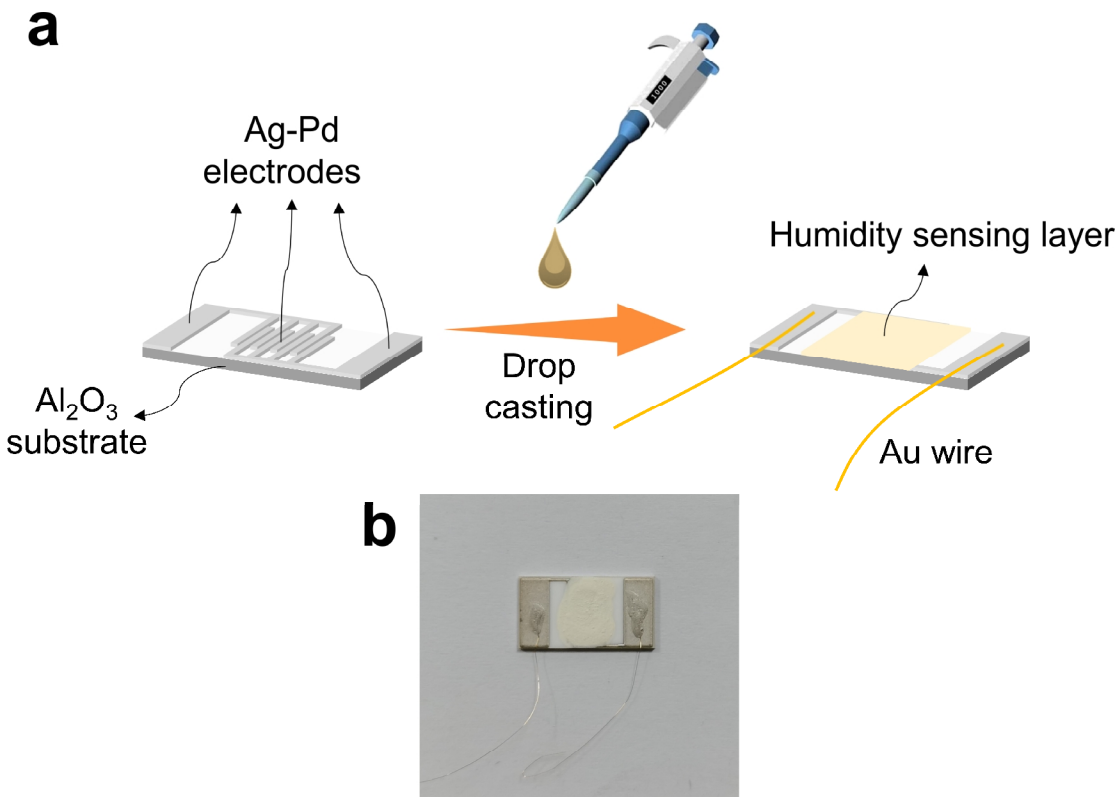

Figure S4. (a) Device structure and its fabrication process, (b) device image.

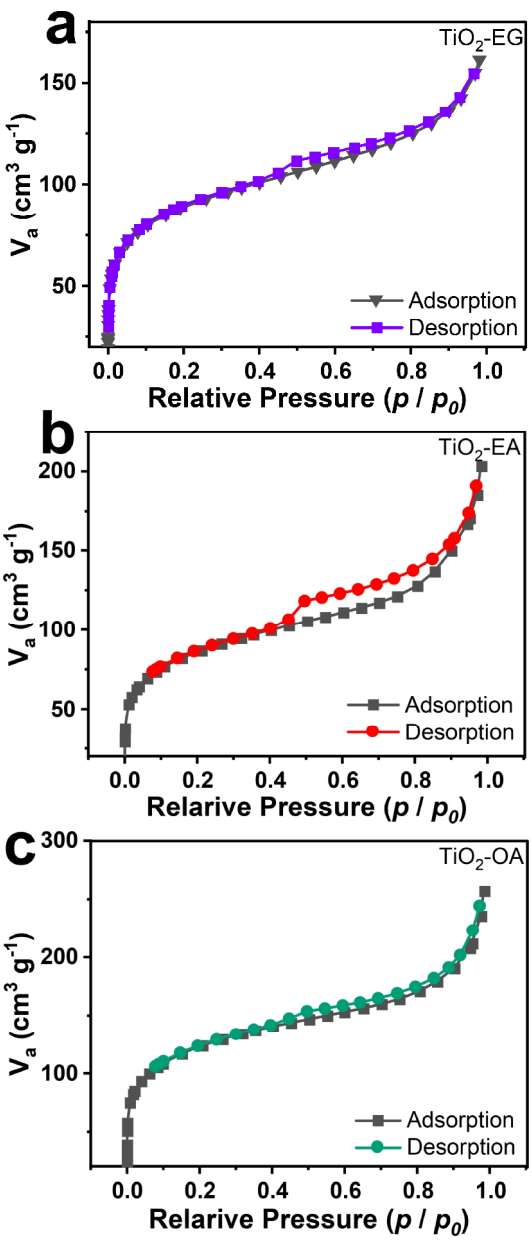

Figure S5. Nitrogen adsorption-desorption isotherms of TiO_2-EG, TiO_2-EA and TiO_2-OA.

The BET surface areas of TiO_2-EG, TiO_2-EA and TiO_2-OA are all about 320 $m^2 \cdot g^{-1}$.

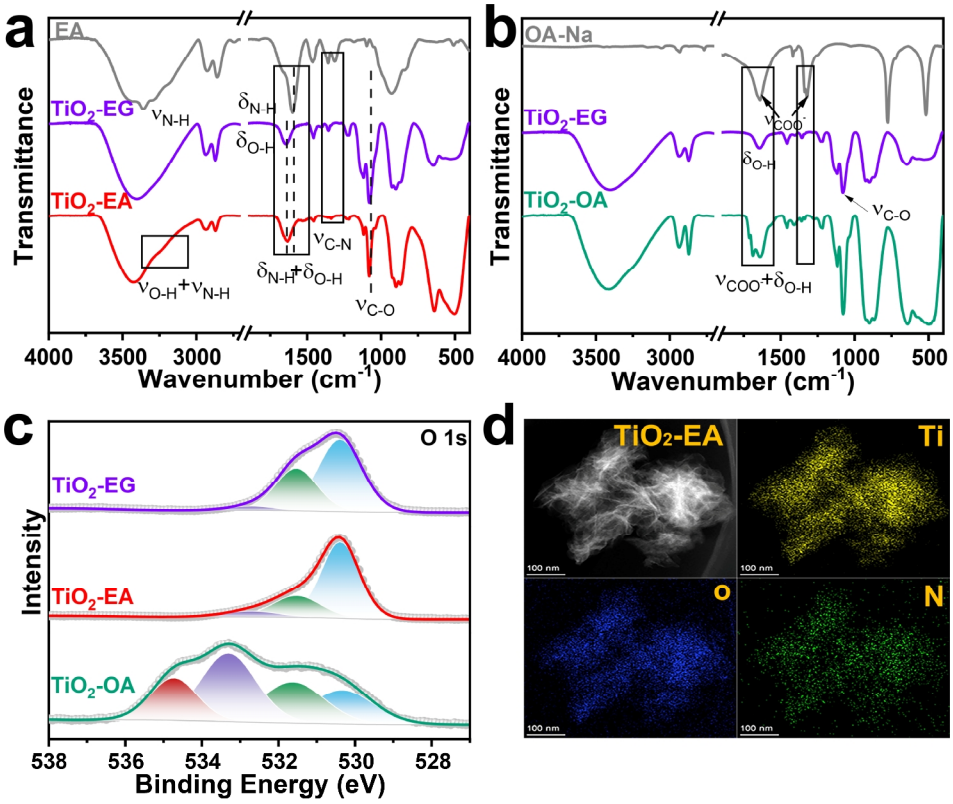

Figure S6. FT-IR spectra of (a) EA and TiO_2(EA) and (b) OA and TiO_2(OA). (b) XPS spectrum of O 1s of TiO_2-EG, TiO_2-EA, and TiO_2-OA

The unmodified TiO_2-EG sample exhibited a strong broad absorption band at around 3408 cm^{-1}. This band could be assigned to the -OH stretching vibrations of the surface coordinated ethylene glycol and physisorbed water molecules. Another strong adsorption band located at 1640 cm^{-1} was attributed to the bending vibration of -OH and adsorbed water. The adsorption band regions on 2935 and 2871 cm^{-1} were assigned to $-CH_2$ stretching vibration of ethylene glycol ligand. And the obvious adsorption bands at about 1078 and 1116 cm^{-1} were assigned to the stretching vibrations of -C-O.

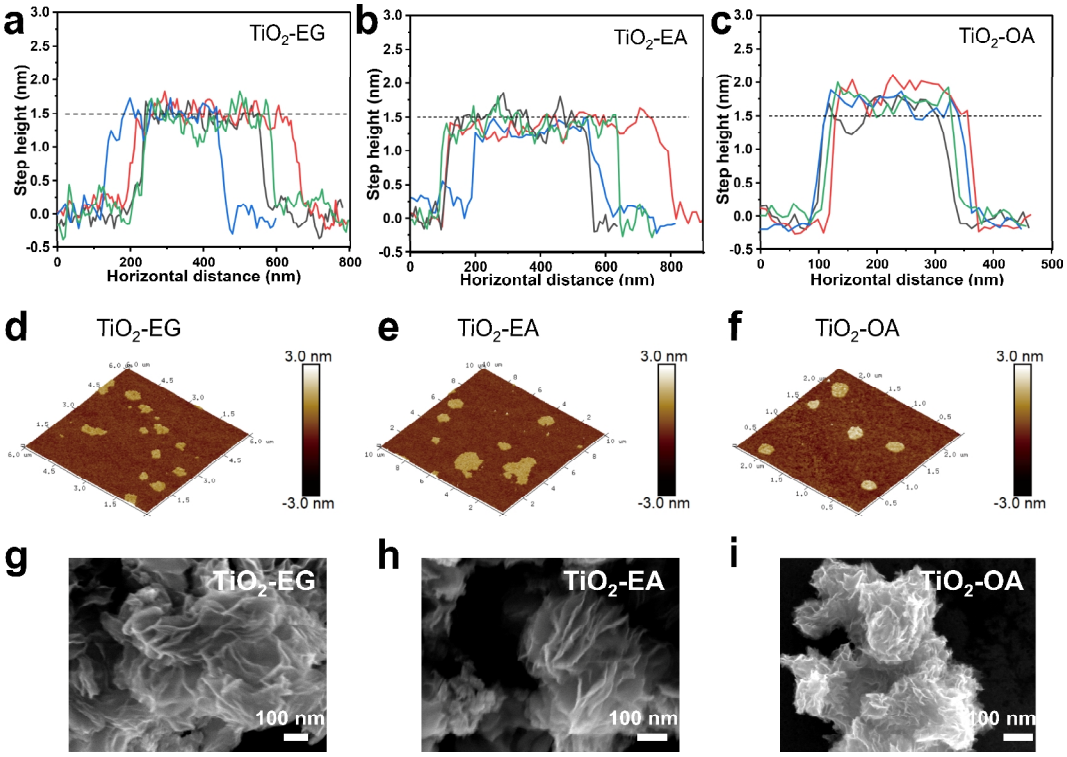

Figure S7. (a)–(f) Thickness of TiO_2-EG, TiO_2-EA, TiO_2-OA; (g)–(i) High-resolution SEM images of TiO_2-EG, TiO_2-EA, and TiO_2-OA.

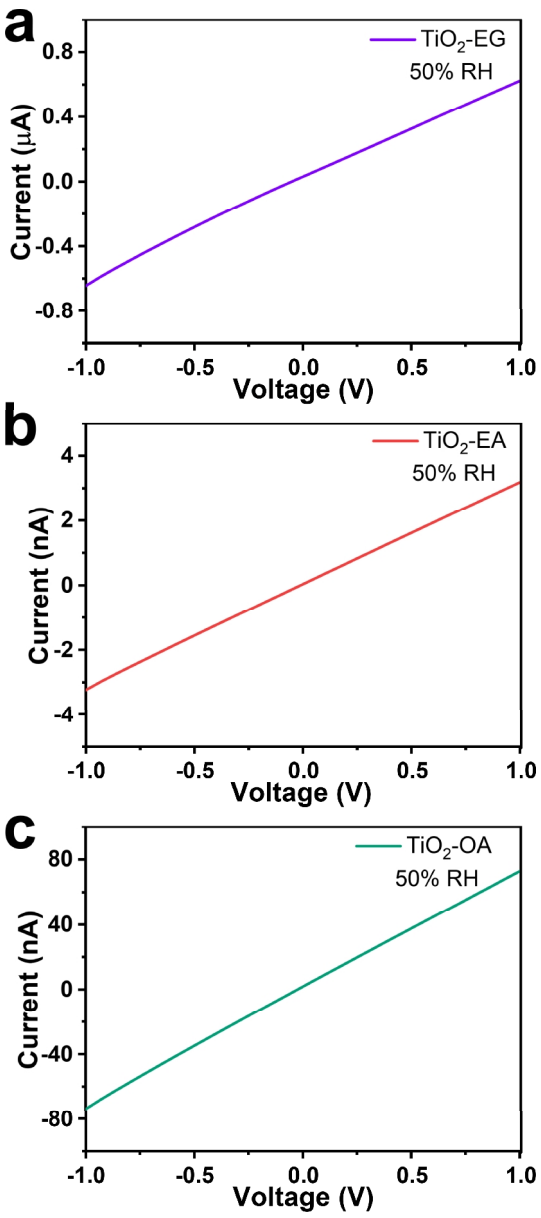

Figure S8. I-V characteristic curve tests of (a) TiO_2-EG, (b) TiO_2-EA, and (c) TiO_2-OA.

The I-V characteristic curve tests of three TiO_2 samples are performed to confirm the contact type between metal and semiconductor, as shown in Figure S5. It can be seen from the results that all the I-V curves obtained are straight lines with slope passing through the origin, indicating that no band bending occurs within the interface between metal and semiconductor, so no Schottky barriers are formed. There are good ohmic contacts between electrode metal and the TiO_2 samples instead of Schottky contacts, and the interface resistances are very small. The current response of the humidity sensor comes from the charge transfer of interaction between the TiO_2 sensor layer and water molecules.

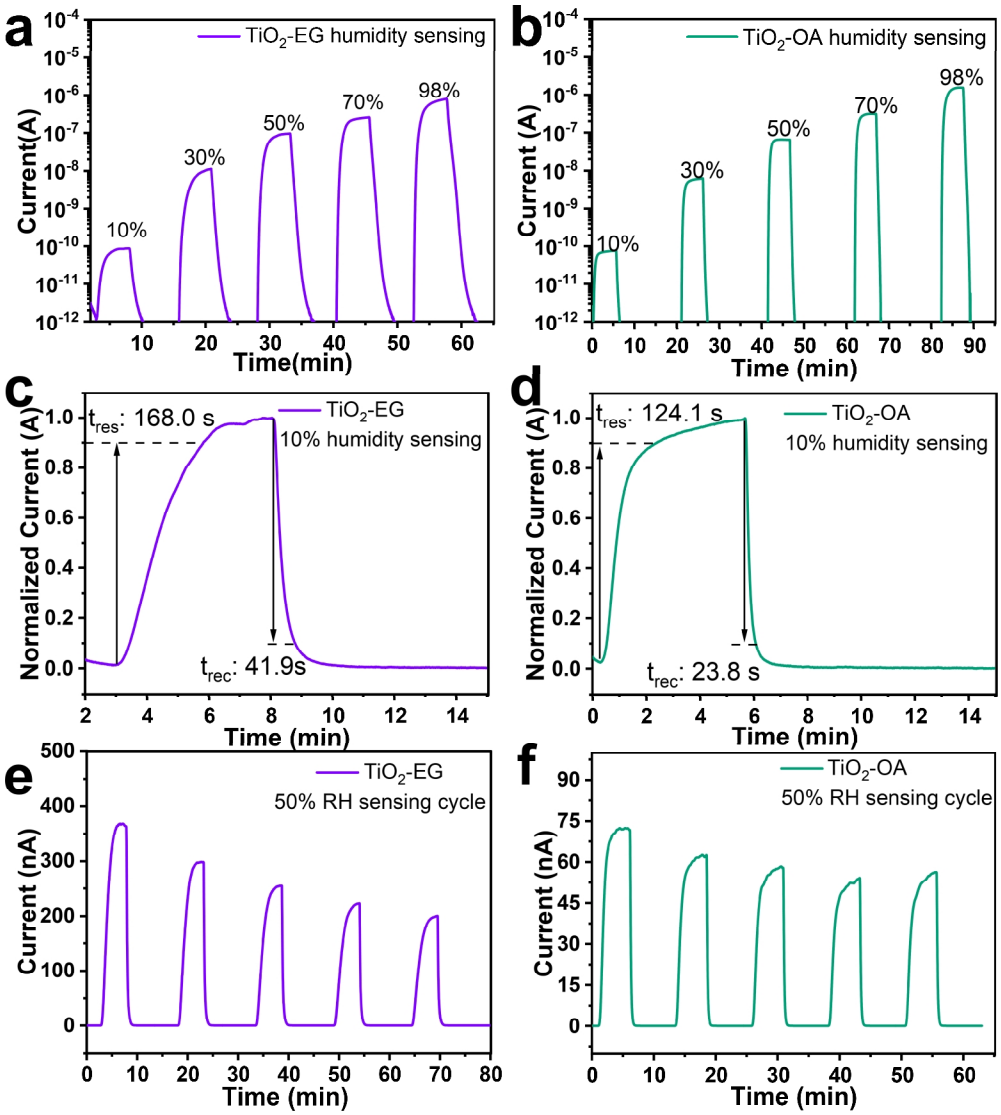

Figure S9. (a), (b) Real-time dynamic current response-recovery plots of TiO_2-EG and TiO_2-OA, (c)–(d) Response-10%RH sensing plots of TiO_2-EG and TiO_2-OA, (e–f) Response-recovery cycle plots of TiO_2-EG and TiO_2-OA at 50%RH.

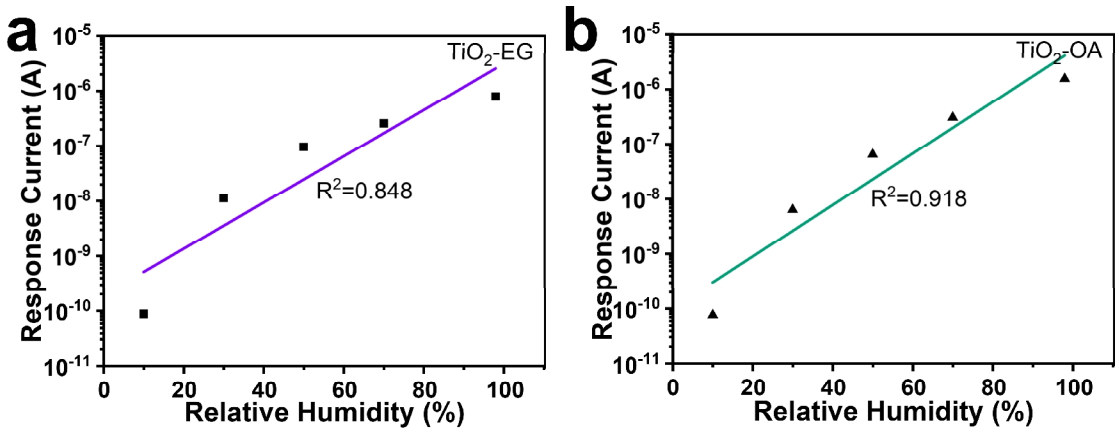

Figure S10. Response current plots of TiO_2-EG and TiO_2-OA at different RH.

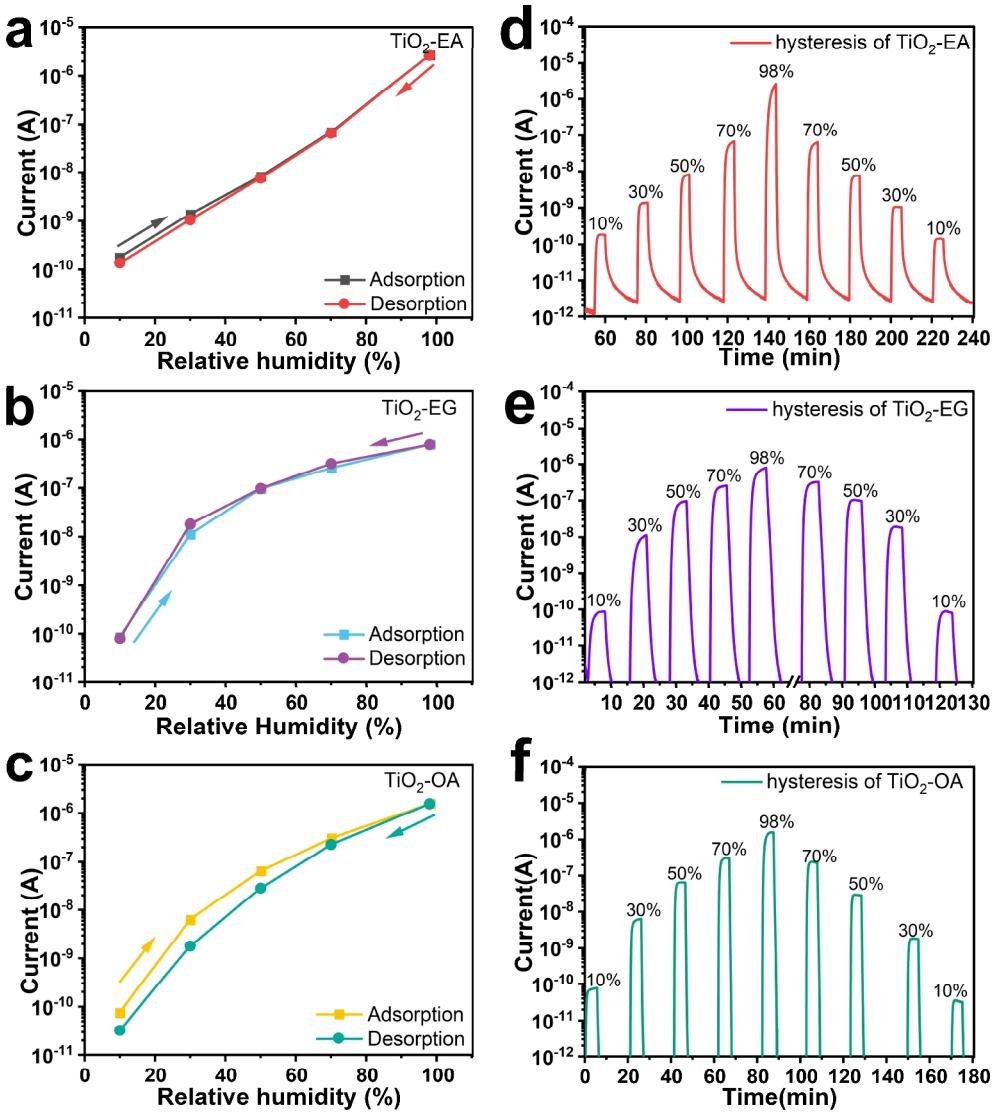

Figure S11. (a)–(c) Hysteresis characteristic of TiO_2-EG, TiO_2-EA, TiO_2-OA; (d)–(f) Dynamic sensing plots of hysteresis measurements of TiO_2-EA, TiO_2-EG, and TiO_2-OA.

Hysteresis characteristic of a humidity sensor is another important criterion for humidity sensing performance, which is defined as the maximum difference during the adsorption-desorption process. It represents the work properties of water molecular adsorption and desorption during the humidity sensing process and is a common phenomenon for metal oxides-based humidity sensing materials. Minimizing the hysteresis effect is an important issue to make the humidity sensing materials be practical. As shown in Figure S5, the TiO_2-EA has the narrowest hysteresis range compared with TiO_2-EG and TiO_2-OA in the whole humidity range of 10–98%, indicating that the sensors fabricated by TiO_2-EA have good reliability and excellent reversibility in humidity sensing application. The excellent performance of the sensors may be due to the atomically thin morphology and the special chemical environment of TiO_2-EA.

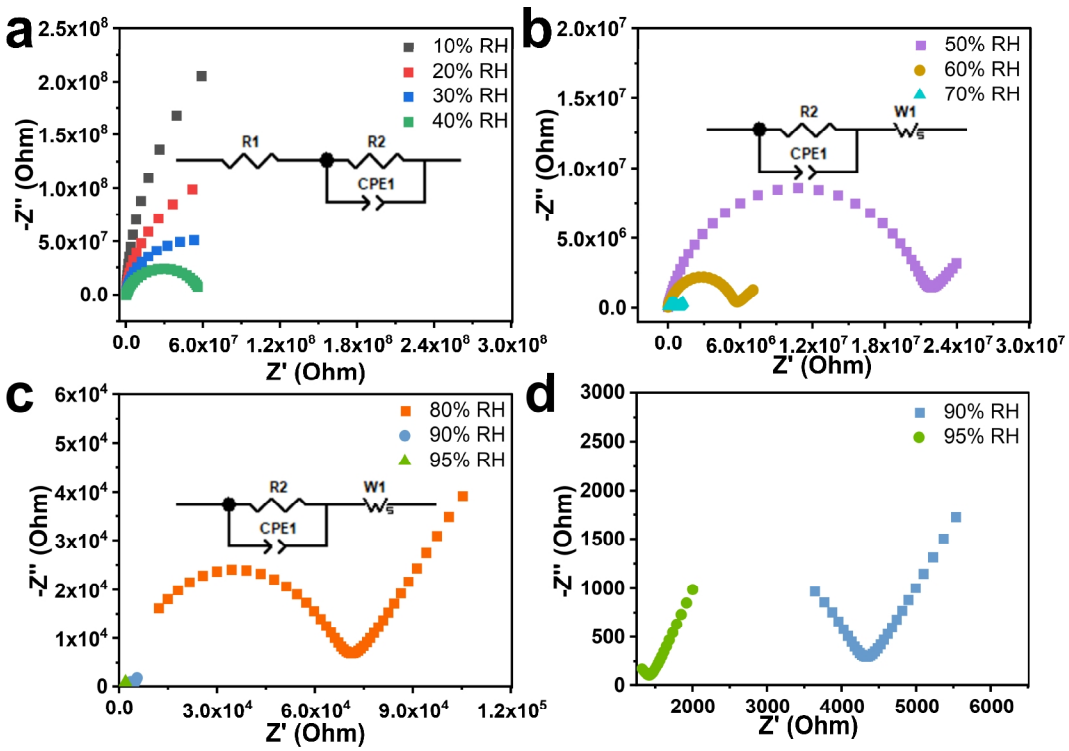

Figure S12. The corresponding equivalent circuit and the fitting plots at different humidity levels.

The equivalent fittings were performed by Z-View 2, and the resultant component values of the equivalent circuit at different humidity levels are listed in Table S2. Compared with the test plots, we can find that the fitting plots match the test plots perfectly, indicating the validity and correctness of the equivalent circuit.

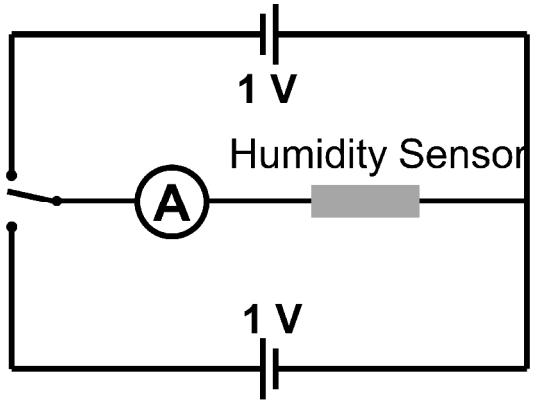

Figure S13. DC circuit of instantaneous reverse polarity experiment.

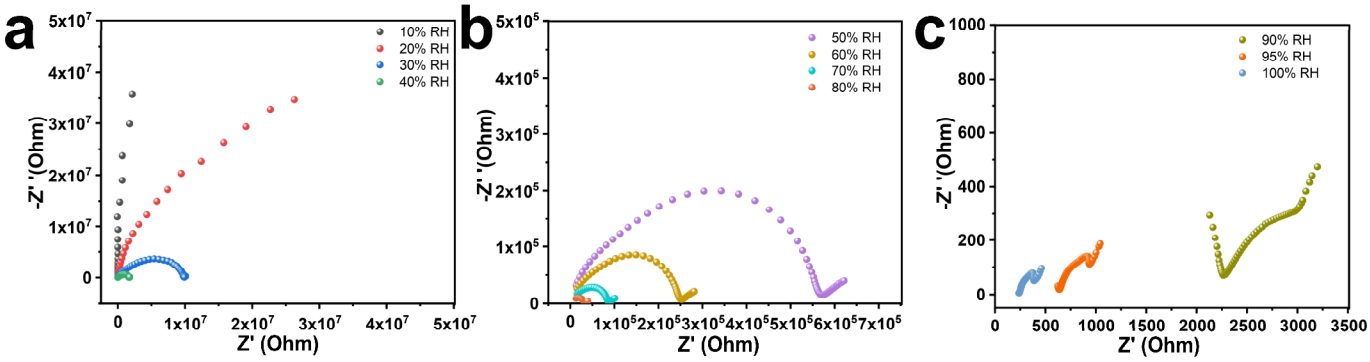

Figure S14. AC impedance spectra of TiO_2-EG at different RH levels.

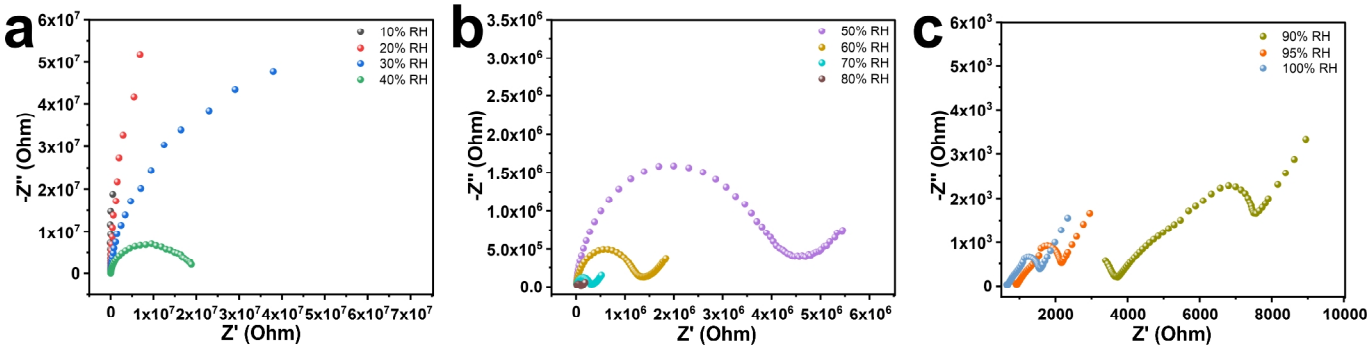

Figure S15. AC impedance spectra of TiO_2-OA at different RH levels.

From the AC impedance spectra of TiO_2-EG and TiO_2-OA at different RH levels, we can see that the ion diffusion phenomenon in high humidity at low frequency is not as good as that of TiO_2-EA, indicating the more complicated process in high humidity sensing.

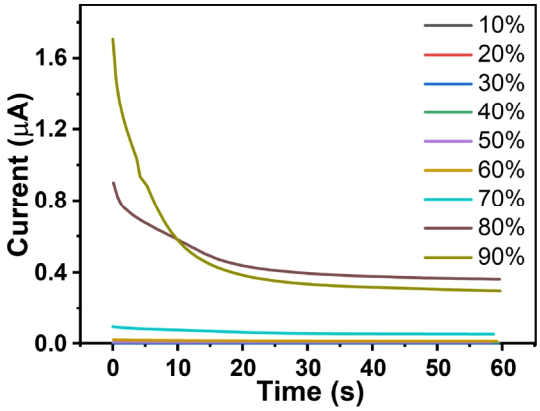

Figure S16. The total DC instantaneous reverse polarity experiment plots of TiO_2-EA from 10% to 90% RH.

Table S1. Comparison of TiO_2-Based Humidity Sensors

Sensing materials	Change in the impedance/resistance	Response time (s)	Recovery time (s)	Ref.
TiO_2 porous ceramic	10^4 (11–95)	32	131	[3]
Porous TiO_2	10^4 (11–95)	5	8	[4]
TiO_2 nanotube	10^2 (11–95)	100	190	[5]
TiO_2 thin film	10^3 (10–95)	10	180	[6]
TiO_2 nanowire/nafion	10^4 (12–76)	<120	<120	[7]
KCl-doped TiO_2 nanofiber	10^4 (11–95)	3	3	[8]
LiCl doped TiO_2 nanofiber	10^3 (11–95)	3	7	[9]
Mg^{2+} and Na^+ doped TiO_2 nanofiber	10^3 (11–95)	1	2	[10]
ZrO_2:TiO_2 hetero-nanofiber	10^4 (11–97)	5	20	[11]
Graphene/TiO_2 composite	10^2 (12–90)	128	68	[12]
TiO_2 nanosheet	10^2 (12–90)	3	50	[13]
TiO_2/($K_{0.5}Na_{0.5}$)NbO_3)	10^2 (12–94)	25	38	[14]
TiO_2 nanoflowers	10 (11–98)	143	33	[15]
TiO_2 slanted nanorods	10^3 (5–95)	0.145	0.21	[16]
Electro spun TiO_2 nanofiber	$<10^3$	1	4	[17]
TiO_2/GO	$<10^2$ (11–97)	0.45	0.89	[18]
ZnO/TiO_2 double-layer nanofibers	10^4 (11–95)	11	7	[19]
TiO_2 nanoparticles	$<10^3$ (11–98)	2	1.5	[20]

Table S2. Comparison of Different Type of Ultra-low Humidity Sensors

Materials	Response time (s)	Recovery time (s)	Operating range (ppm)	Sensor type	Ref.
Au layer/MEH-PPV	120	600	1–5000	Resistive type	[21]
Polyaniline	520	30	≥11.5	Resistive type	[22]
FDU-15-COOH	/	/	55–2952	QCM type	[23]
CNT/Nafion composite	<5	<5	8.5–15300	QCM type	[24]
NiI_2	/	/	111–3070	Impedance type	[25]
H-ZSM-5 type zeolite	/	/	10–110	Impedance type	[26]
PEDOT: PSS	/	/	<278	Impedance type	[27]
QC-P4VP/RGO	21	78	50–585	Impedance-type	[28]
Al_2O_3 modified MCL	≥120	160	10–200	MCL type	[29]
γ-Al_2O_3	67	121	278–2789	Capacitive type	[30]
γ-Al_2O_3	30	40	4–18	Capacitive type	[31]
γ-Al_2O_3	47	118	2.5–25	Capacitive type	[32]
γ-Al_2O_3	158	216	3.5–800	Capacitive type	[33]
γ-Al_2O_3	12	12	175–625	Capacitive type	[34]
γ-Al_2O_3	158	216	3.5–800	Capacitive type	[35]
γ-Al_2O_3	/	/	0–100	Capacitive type	[36]
Cu–BTC	<480	<420	20–100	Capacitive type	[37]
Anodic spark Al_2O_3	5	5	0–23000	Capacitive type	[38]
Ultra-thin TiO_2 nanosheet	98.4	93.6	15–28028	Chemiresistive type	This work

Table S3

RH	R_1(Ω)	R_2 (Ω)	CPE_1-T (Ω)	CPE_1-P (Ω)	W_1-R (Ω)	W_1-T (Ω)	W_1-P (Ω)
10%	3510	8.6×10^{8}	5.1×10^{12}	0.98	/	/	/
20%	2418	2.7×10^{9}	6.3×10^{-12}	0.97	/	/	/
30%	843	1.1×10^{9}	8.8×10^{-12}	0.95	/	/	/
40%	/	5.8×10^{7}	1.9×10^{-11}	0.89	/	/	/
50%	/	2.7×10^{7}	3.8×10^{-11}	0.86	6.7×10^{14}	6.1×10^{14}	0.53
60%	/	5.4×10^{6}	4.6×10^{-11}	0.85	2.0×10^{13}	5.2×10^{15}	0.42
70%	/	8.0×10^{5}	8.5×10^{-11}	0.82	4.3×10^{7}	1151	0.44
80%	/	6.8×10^{4}	2.5×10^{-10}	0.77	2.9×10^{5}	0.06	0.52
90%	/	4210	3.4×10^{-10}	0.78	5.6×10^{11}	1.5×10^{10}	0.59
95%	/	1416	1.7×10^{-9}	0.70	7.9×10^{11}	2.2×10^{9}	0.66

n REFERENCE

(1) Xiang, G.; Li, T.; Zhuang, J.; Wang, X. Large-scale synthesis of metastable TiO_2(B) nanosheets with atomic thickness and their photocatalytic properties. *Chem. Commun. (Camb.)* **2010**, 46, 6801–6803.
(2) Yao, M. S.; Tang, W. X.; Wang, G. E.; Nath, B.; Xu, G. MOF thin film-coated metal oxide nanowire array: significantly improved chemiresistor sensor performance. *Adv. Mater.* **2016**, 28, 5229–5234.
(3) Wang, X.; Li, J. H.; Li, Y. I.; Liu, L. J.; Guan, W. M. Emulsion-templated fully three-dimensional interconnected porous titania ceramics with excellent humidity sensing properties. *Sens. Actuators, B* **2016**, 237, 894–898.
(4) Wang, Z.; Shi, L.; Wu, F.; Yuan, S.; Zhao, Y.; Zhang, M. The sol-gel template synthesis of porous TiO_2 for a high performance humidity sensor. *Nanotechnology* **2011**, 22, 275502.
(5) Zhang, Y.; Fu, W.; Yang, H.; Qi, Q.; Zeng, Y.; Zhang, T.; Ge, R.; Zou, G. Synthesis and characterization of TiO_2 nanotubes for humidity sensing. *Appl. Surf. Sci.* **2008**, 254, 5545–5547.
(6) Biju, K. P.; Jain, M. K. Effect of polyethylene glycol additive in sol on the humidity sensing properties of a TiO_2 thin film. *Meas. Sci. Technol.* **2007**, 18, 2991.
(7) Wu, R. J.; Sun, Y. L.; Lin, C. C.; Chen, H. W.; Chavali, M. Composite of TiO_2 nanowires and Nafion as humidity sensor material. *Sens. Actuators, B* **2006**, 115, 198–204.
(8) Qi, Q.; Feng, Y.; Zhang, T.; Zheng, X.; Lu, G. Influence of crystallographic structure on the humidity sensing properties of KCl-doped TiO_2 nanofibers. *Sens. Actuators, B* **2009**, 139, 611–617.
(9) Li, Z.; Zhang, H.; Zheng, W.; Wang, W.; Huang, H.; Wang, C.; MacDiarmid, A. G.; Wei, Y. Highly sensitive and stable humidity nanosensors based on LiCl doped TiO_2 electrospun nanofibers. *J. Am. Chem. Soc.* **2008**, 130, 5036–5037.
(10) Zhang, H.; Li, Z.; Liu, L.; Wang, C.; Wei, Y.; MacDiarmid, A. G. Mg^{2+}/Na^{+}-doped rutile TiO_2 nanofiber mats for high-speed and anti-fogged humidity sensors. *Talanta* **2009**, *79*, 953–958.
(11) Su, M.; Wang, J.; Du, H.; Yao, P.; Zheng, Y.; Li, X. Characterization and humidity sensitivity of electrospun ZrO_2: TiO_2 hetero-nanofibers with double jets. *Sens. Actuators, B* **2012**, 161, 1038–1045.
(12) Lin, W. D.; Liao, C. T.; Chang, T. C.; Chen, S. H.; Wu, R. J. Humidity sensing properties of novel graphene/TiO_2 composites by sol-gel process. *Sens. Actuators, B* **2015**, 209, 555–561.
(13) Gong, M.; Li, Y.; Guo, Y.; Lv, X.; Dou, X. 2D TiO_2 nanosheets for ultrasensitive humidity sensing application benefited by abundant surface oxygen vacancy defects. *Sens. Actuators, B* **2018**, 262, 350–358.
(14) Si, R.; Xie, X.; Li, T.; Zheng, J.; Cheng, C.; Huang, S.; Wang, C. TiO_2/(K, Na) NbO_3 nanocomposite for boosting humidity-sensing performances. *ACS sensors* **2020**, 5, 1345–1353.
(15) Shinde, P. V.; Gagare, S.; Rout, C. S.; Late, D. J. TiO_2 nanoflowers based humidity sensor and cytotoxic activity. *RSC Adv.* **2020**, 10, 29378–29384.
(16) Jyothilal, H.; Shukla, G.; Walia, S.; Kundu, S.; Angappane, S. Humidity sensing and breath analyzing applications of TiO_2 slanted nanorod arrays. *Sens. Actuators, A* **2020**, 301, 111758.
(17) Jamil, H.; Batool, S. S.; Imran, Z.; Usman, M.; Rafiq, M.; Willander, M.; Hassan, M. Electrospun titanium dioxide nanofiber humidity sensors with high sensitivity. *Ceram. Int.* **2012**, 38, 2437–2441.
(18) Zhao, X.; Chen, X.; Yu, X.; Ding, X.; Yu, X.; Chen, X. Fast response humidity sensor based on graphene oxide films supported by TiO_2 nanorods. *Diamond Relat. Mater.* **2020**, 109, 108031.
(19) Yue, X. J.; Hong, T. S.; Xu, X.; Li, Z. High-performance humidity sensors based on double-layer ZnO-TiO_2 nanofibers via electrospinning. *Chin. Phys. Lett.* **2011**, 28, 090701.
(20) Poonia, E.; Mishra, P. K.; Kiran, V.; Sangwan, J.; Kumar, R.; Rai, P. K.; Tomer, V. K. Aero-gel assisted synthesis of anatase TiO_2 nanoparticles for humidity sensing application. *Dalton Trans.* **2018**, 47, 6293–6298.
(21) Hossein-Babaei, F.; Shabani, P. A gold/organic semiconductor diode for ppm-level humidity sensing. *Sens. Actuators, B* **2014**, 205, 143–150.
(22) Joulazadeh, M.; Navarchian, A. H.; Niroomand, M. A comparative study on humidity sensing performances of polyaniline and polypyrrole nanostructures. *Adv. Polym. Technol.* **2014**, 33, 21461.
(23) Zhu, Y.; Zhang, W.; Xu, J. Preparation of functional ordered mesoporous carbons and their application as the QCM sensor with ultra-low humidity. *Chin. Chem. Lett.* **2020**, 31, 2150–2154.
(24) Chen, H. W.; Wu, R. J.; Chan, K. H.; Sun, Y. L.; Su, P. G. The application of CNT/Nafion composite material to low humidity sensing measurement. *Sens. Actuators, B* **2005**, 104, 80–84.
(25) Zhang, Y.; Ren, J.; Wu, Y.; Zhong, X.; Luo, T.; Cao, J.; Yin, M.; Huang, M.; Zhang, Z. Application of moisture-induced discoloration material nickel(II) iodide in humidity detection. *Sens. Actuators, B* **2020**, 309, 127769.
(26) Neumeier, S.; Echterhof, T.; Bolling, R.; Pfeifer, H.; Simon, U. Zeolite based trace humidity sensor for high temperature applications in hydrogen atmosphere. *Sens. Actuators, B* **2008**, 134, 171–174.
(27) Hossein-Babaei, F.; Akbari, T.; Harkinezhad, B. Dopant passivation by adsorbed water monomers causes high humidity sensitivity in PEDOT: PSS thin films at ppm-level humidity. *Sens. Actuators, B* **2019**, 293, 329–335.
(28) Li, Y.; Fan, K.; Ban, H.; Yang, M. Detection of very low humidity using polyelectrolyte/graphene bilayer humidity sensors. *Sens. Actuators, B* **2016**, 222, 151–158.
(29) Shi, X.; Chen, Q.; Fang, J.; Varahramyan, K.; Ji, H. F. Al_2O_3-coated microcantilevers for detection of moisture at ppm level. *Sens. Actuators, B* **2008**, 129, 241–245.
(30) Saha, D.; Das, S.; Sengupta, K. Development of commercial nanoporous trace moisture sensor following sol-gel thin film technique. *Sens. Actuators,*

B **2008**, 128, 383–387.
(31) Pandey, M.; Mishra, P.; Saha, D.; Sengupta, K.; Jain, K.; Islam, S. S. Nanoporous alumina (γ- and α-phase) gel cast thick film for the development of trace moisture sensor. *J. Sol-gel Sci. Technol.* **2013**, 68, 317–323.
(32) Islam, T.; Kumar, L.; Khan, S. A. A novel sol-gel thin film porous alumina based capacitive sensor for measuring trace moisture in the range of 2.5–25 ppm. *Sens. Actuators, B* **2012**, 173, 377–384.
(33) Islam, T.; Khan, A. U.; Akhtar, J.; Rahman, M. Z. U. A digital hygrometer for trace moisture measurement. *IEEE Trans. Ind. Electron.* **2014**, 61, 5599–5605.
(34) Islam, T.; Nimal, A. T.; Mittal, U.; Sharma, M. U. A micro interdigitated thin film metal oxide capacitive sensor for measuring moisture in the range of 175–625 ppm. *Sens. Actuators, B* **2015**, 221, 357–364.
(35) Islam, T.; Mahboob, M. R.; Khan, S. A. A Simple MOX vapor sensor on polyimide substrate for measuring humidity in ppm level. *IEEE Sensors Journal* **2015**, 15, 3004–3013.
(36) Mistry, K. K.; Saha, D.; Sengupta, K. Sol-gel processed Al_2O_3 thick film template as sensitive capacitive trace moisture sensor. *Sens. Actuators, B* **2005**, 106, 258–262.
(37) Hosseini, M. S.; Zeinali, S. Capacitive humidity sensing using a metal-organic framework nanoporous thin film fabricated through electrochemical in situ growth. *J. Mater. Sci.: Mater. Electron.* **2019**, 30, 3701–3710.
(38) Chen, Z.; Lu, C. Humidity sensors: a review of materials and mechanisms. *Sens. Lett.* **2005**, 3, 274–295.